Journal of
Synchrotron Radiation

ISSN 0909-0495

Received 14 November 2004
Accepted 20 May 2005

Studying morphological variations across single fibres using an X-ray waveguide

Richard J. Davies,* Manfred Burghammer and Christian Riekel

European Synchrotron Radiation Facility, BP 220, F-38043 Grenoble CEDEX, France.
E-mail: rdavies@esrf.fr

Waveguide and glass capillary optics have been used to study morphological variations across single as-spun poly(*p*-phenylene benzobisoxazole) (PBO) fibres. The waveguide provides a beam with a submicrometre dimension perpendicular to the fibre axis. The glass capillary optics provide a beam of a few micrometres in diameter. By directly comparing results obtained with both optics it is possible to assess the influence of beam size on experimental observations. The study demonstrates that submicrometre beams are invaluable for detailed morphological studies across single fibres. The greater morphological averaging inherent to data collected using glass capillary optics reduces the variation between skin and core measurements, as well as obscuring other important features. Crystalline domain orientation, (200) crystal plane spacings and reflection intensities can be determined from data generated using a submicrometre beam. All parameters are found to vary significantly across the diameter of single PBO fibres. In terms of orientation, both skin and core regions exhibit a lower degree of crystalline domain orientation than an intermediate zone. In terms of (200) crystal plane spacing, the observed variations suggest residual stresses within the fibre structure following manufacture.

Keywords: waveguide; PBO; skin–core; fibre morphology.

1. Introduction

Many third-generation synchrotron sources are now able to offer high-brilliance microbeams as a matter of routine. This has made microbeam scanning experiments a popular tool for materials characterization. Such experiments typically involve scanning a sample through the beam to produce a series of spatially offset diffraction patterns. The spatial resolution is usually determined by the dimensions of the beam. This has driven the development of beamline optics towards the production of ever-smaller microbeams. At the present time there are several different means of obtaining X-ray beams with a submicrometre dimension on at least one axis. These include KB mirrors (Hignette *et al.*, 2003), Fresnel zone plates (Lai *et al.*, 1998; David *et al.*, 2002) and X-ray waveguides (Jark *et al.*, 1996). For small sample volumes, one-dimensional X-ray waveguide optics offer perhaps the most convenient solution. This is because they provide a means of obtaining a high spatial resolution without sacrificing scattering intensity. A typical beam from an X-ray waveguide has a very high aspect ratio. Thus the beam may be 100–200 nm along one axis whilst being several micrometres along the other axis. For materials which are homogeneous along at least one axis, this provides an effective spatial resolution of 100–200 nm.

Fibre diffraction experiments are an ideal application for the use of waveguide optics. Fibres are generally considered to be axially homogeneous; however, they often exhibit significant structural variations across the fibre diameter (Panar *et al.*, 1983; Morgan *et al.*, 1983; Li *et al.*, 1993; Davies *et al.*, 2003; Riekel *et al.*, 1999; Rebouillat *et al.*, 1999). This radial anisotropy is termed 'skin–core' morphology and arises during fibre manufacture (Morgan *et al.*, 1983; Davies *et al.*, 2003). Such heterogeneities are important for a variety of reasons. For example, they are thought to influence fibre mechanical properties (Young *et al.*, 1992; Graham *et al.*, 2000). Additionally, using localized investigative techniques, the results obtained from radially anisotropic fibres cannot be assumed to represent bulk fibre morphology. This latter point is of particular importance for mechanical modelling where existing models assume both radial and axial fibre homogeneity (Northolt, 1980; Baltussen & Northolt, 1999). Any technique which is capable of investigating such morphological variations is therefore important. There are several non-X-ray methods currently available for probing fibre skin–core morphology. These include atomic force microscopy (AFM), scanning electron microscopy (SEM), interfacial force microscopy (IFM) and selected-area electron diffraction (SAED). Such techniques are often complicated by the

requirement of thin sample sectioning and/or the application of conductive coatings. This significantly increases the risk of artefact induction (Muller *et al.*, 2000). Additionally, electron diffraction methods are often limited by extensive damage during sample exposure to the electron beam (Martin & Thomas, 1991). With the increasing availability of X-ray microbeams, microfocused X-ray diffraction (μ-XRD) is becoming a routine alternative (Davies *et al.*, 2003; Riekel *et al.*, 1999; Roth *et al.*, 2003). μ-XRD does not require sample modification and, for high-performance fibres, sample damage through beam exposure is negligible. Many previous μ-XRD studies on single fibres have been conducted using glass capillary optics (Davies *et al.*, 2001, 2003). These provide an across-fibre beam profile of approximately 3 μm. On a 12 μm fibre such a beam spans 25% of the total fibre diameter. By contrast, a 0.2 μm waveguide beam only spans approximately 1.6% of a 12 μm fibre diameter. Waveguide optics therefore offer more than an order of magnitude increase in effective spatial resolution over glass capillary optics.

In order to highlight the benefits realised by using smaller X-ray beams for fibre diffraction, this study reports on diffraction performed using both waveguide and glass capillary optics. Across-fibre variations in reflection position, reflection intensity and azimuthal broadening will be monitored in order to assess variations in lattice spacing, radial texturing and crystalline domain orientation. By investigating such skin–core morphological variations on the same fibre type using different optics, the influence of beam size on experimental results can be directly investigated. Such comparisons are already significant in assessing the results of X-ray studies against electron diffraction studies. With the future trend towards smaller μ-XRD beam sizes, the validity of comparing existing and future data sets is of prime importance. The data obtained in this study from waveguide optics will also be used to investigate skin–core fibre morphology and relate morphological variations to processing.

2. Experimental

2.1. Materials

A commercial-grade of as-spun (AS) poly(*p*-phenylene benzobisoxazole) (PBO) fibre is investigated in this study. This fibre type is produced by Toyobo (Japan) under the trade name Zylon (AS). The production process involves dry-jet wet-spinning the fibre from a nematic dope through an air gap. Coagulation occurs in an aqueous solution, followed by a tension drying process (Kitagawa *et al.*, 1998, 2001; Choe & Kim, 1981; Kumar, 1990; Wolfe, 1988). This particular fibre type has been chosen as it is known to exhibit significant skin–core morphological variations owing to the fact that it is not heat-treated. Previous studies report that the heat-treatment process decreases across-fibre variations (Davies *et al.*, 2001). The tensile modulus and strength of PBO AS are approximately 180 GPa and 5.5 GPa, respectively (Kitagawa *et al.*, 1998). The polymeric repeat unit of the PBO molecule is shown in Fig. 1.

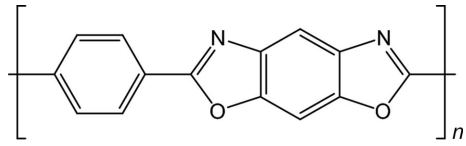

Figure 1
Polymeric repeat unit of the PBO molecule (Kumar, 1990).

2.2. μ-XRD on single PBO fibres

All μ-XRD was carried out at the ESRF on the microfocus beamline (ID13). Experiments were conducted over two separate experimental periods, one employing waveguide optics and one utilizing glass capillary optics. Ideally, precisely the same fibre specimen and region on the fibre would be assessed in both experiments. However, owing to differences in the sample geometries required for the two different optics, this was not feasible. Consequently, it should be noted that two different fibre specimens of the same fibre type were employed for each experiment. Whilst this may not be ideal, it is not thought to be a significant limitation for this particular experiment. For instance, the as-spun fibre type under study has not been heat-treated and therefore processing history variations between filaments are minimal. A brief summary of both experimental set-ups is given below with more detailed information provided elsewhere (Davies *et al.*, 2001, 2003; Roth *et al.*, 2003).

For the experiment conducted using X-ray waveguide optics, a short length of PBO fibre was adhered to the end of a glass capillary and mounted on the beamline positioning stage. The fibre was aligned so that the longer axis of the waveguide beam was parallel to the fibre axis. This beam dimension is defined by the beam profile entering the waveguide and was approximately 3 μm in this instance. The dimension of the beam perpendicular to the fibre axis was approximately 0.1 μm at the waveguide exit (Roth *et al.*, 2003; Jark *et al.*, 1996). The experiment was performed using the TE_0 mode of the waveguide with a divergence of approximately 1 mrad (Roth *et al.*, 2003; Jark *et al.*, 1996). With the fibre positioned as close to the exit of the waveguide as possible, the actual across-fibre beam size cannot be larger than 0.2 μm (Roth *et al.*, 2003). Diffraction patterns were generated across the as-spun PBO fibre at 0.2 μm intervals by moving the fibre through the beam. Thus a series of diffraction patterns covering the entire fibre diameter were obtained.

For the experiment employing glass capillary optics, the PBO fibre was mounted under minimal tension (sufficient only to stabilize the sample in the beam) on the beamline positioning stage. The optics consist of a collimating glass capillary and a defining aperture. This provides a beam spot size of approximately 3 μm on the fibre sample. Diffraction patterns were obtained across the fibre at 2 μm intervals by moving the fibre through the beam. Again, a series of diffraction patterns were obtained covering the entire fibre diameter.

Fig. 2 shows a schematic representation of both the waveguide and glass capillary beam profiles superimposed proportionally onto an SEM micrograph of a single PBO fibre. During both experiments diffraction patterns were collected

on a MARCCD detector with an average pixel resolution of 64.45 μm^2. The exposure times were 30 s in both instances, with a radiation wavelength of approximately 0.97 Å.

2.3. Data treatment

Diffraction data analysis was performed using a combination of the *Fit2D* software application (Hammersley *et al.*, 1994, 1995) and a custom-written automated analysis application. The latter application was used for the automated generation of macros for processing in *Fit2D*. It was also employed to perform batched function fitting, and orientation and integration operations to the radial and azimuthal intensity profiles. Prior to analysis, a background image was first subtracted from each diffraction pattern. This was necessary to reduce the influence of air scattering and also remove intensity artefacts caused by the use of waveguide optics. The subtraction was scaled to account for any variations in beam brilliance. Fig. 3 shows a comparison between typical diffraction patterns obtained from PBO AS fibres using both waveguide and glass capillary optics. Variations in reflection positions can be attributed to slightly different sample-to-film distances between experiments. All reflections have been indexed after Fratini *et al.* (1989). Note that the apparent lack of a 006 meridional reflection in the lower hemisphere of the waveguide data in Fig. 3 is actually due to part of the experimental set-up shading the detector.

In this study the degree of crystalline domain orientation is expressed in terms of the common $\langle \sin^2\theta \rangle$ orientation parameter. This is calculated from azimuthal broadening of the 200 equatorial reflection, as described in previous studies (Davies *et al.*, 2003). The calculation requires a radial integration around the position of maximum scattering intensity in order to obtain azimuthal profiles. A fitted Lorentz IV function was used for the calculation of $\langle \sin^2\theta \rangle$, a more detailed account of which is given elsewhere (Davies *et al.*, 2003; Northolt, 1980; Northolt & VanAartsen, 1977). Fig. 4 shows a typical example of a Lorentz IV fit to the azimuthal intensity profile of the 200 equatorial reflection. The Lorentz IV function provides a good fit to the experimental data for highly oriented fibres such as PBO.

To determine variations in across-fibre reflection intensity, the 200 equatorial reflection was used. The intensity of the reflection was determined for each diffraction pattern by integrating the Lorentz IV function fitted to the azimuthal intensity profile. This method accounts for possible intensity variations arising through differences in domain orientation. To determine crystal lattice spacings (*d*-spacings) of (200) crystal planes, the radial position of the 200 equatorial

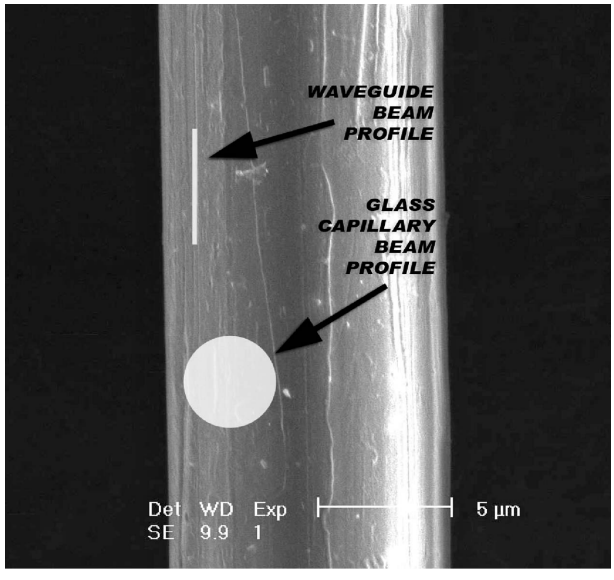

Figure 2
A comparison of glass capillary and waveguide beam profiles superimposed to scale on an SEM micrograph of a PBO fibre.

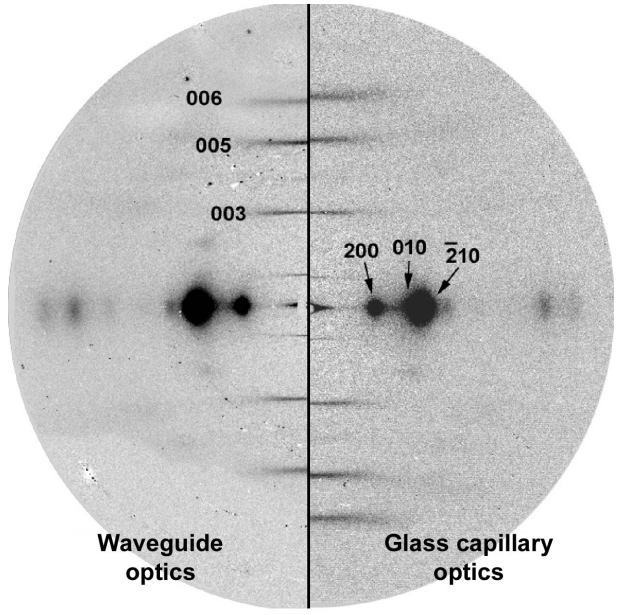

Figure 3
Comparison of PBO diffraction patterns obtained using waveguide (left hemisphere) and glass capillary (right hemisphere) optics.

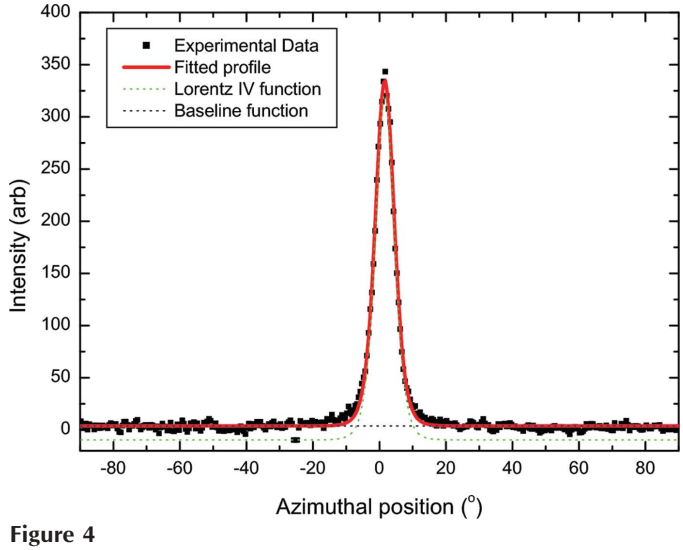

Figure 4
Example of Lorentz IV function fitting to the azimuthal profile of the 200 equatorial reflection of PBO AS.

reflection was determined. For each diffraction pattern the radial intensity profile was fitted using Lorentzian functions. This is shown in Fig. 5, which demonstrates the good correlation between the fitted Lorentzian functions and the experimental data. Crystal lattice spacings (*d*-spacings) were calculated from the position of the 200 reflection using the Bragg equation. For convenience, the results in this study are expressed in terms of the change in lattice spacing (ΔÅ) as a function of beam position across the fibre.

3. Results

3.1. Crystalline domain orientation

Fig. 6 shows the variation in crystalline domain orientation across single PBO AS fibres. Data series representing both glass capillary and waveguide optics are shown for comparison. Overall the two series are in general agreement with both results indicating a higher orientation parameter in the fibre skin and core regions. Calculating the average orientation parameter also yields similar values between series. These are $\langle\sin^2\theta\rangle = 0.0074$ and $\langle\sin^2\theta\rangle = 0.0077$ for waveguide and glass capillary data, respectively. This excellent agreement validates the comparison of two different fibres and demonstrates that no gross morphological differences are likely to exist between them. Thus variations between experimental series can be attributed solely to differences in beam size with some confidence. In Fig. 6 the variation in orientation parameter between skin and core is clearly beam-size dependent. The range of values obtained for the waveguide data series is more than double that of the glass capillary series. Therefore, reducing the across-fibre beam profile permits a greater range in variations to be measured. This is through a reduction in the amount of morphological averaging occurring at each beam position. Such a conclusion is self-evident considering that averaging serves to smooth out extreme values. Increasing the across-fibre beam dimension effectively increases the apparent homogeneity of the fibre under study.

If fibre morphology is now considered, both data series indicate the fibre core region to exhibit a lower degree of crystalline domain orientation (higher orientation parameter). This result is in agreement with a previous μ-XRD study on PBO AS (Davies *et al.*, 2003). However, both series also show an increased orientation parameter in the fibre skin region which was not previously reported (Davies *et al.*, 2003). These variations are most evident in the waveguide data where there is less morphological averaging. This explains why the previous μ-XRD study of as-spun PBO using glass capillary optics did not report this particular feature (Davies *et al.*, 2003). In this case it was not certain whether the increase in skin orientation parameter was an artefact caused by the decreasing material volume at the extremities of the fibre. In light of the waveguide data presented in Fig. 6, the possibility of an artefact can be excluded. Thus for PBO AS, the highest degree of crystalline domain orientation is within an intermediate region, between fibre skin and core. The lower degree of crystalline domain orientation in the fibre core has previously been attributed to shear forces generated during the spinning process. These forces are thought to result in a preferential alignment of the crystalline domains in contact with the walls of the spinneret (Davies *et al.*, 2003). Whilst this hypothesis seems to be a reasonable explanation for the lower orientation in the fibre core, it fails to explain why a lower orientation is also observed in the fibre skin region. Indeed, based upon such a hypothesis, the fibre skin may be expected to exhibit the highest degree of crystalline domain orientation. Evidently there must be other mechanisms which strongly influence crystalline domain orientation during fibre manufacture.

A previous IFM study of poly(*p*-phenylene terephthalamide) (PPTA) fibres reports that the skin region of PPTA exhibits a much lower elastic modulus than the core region (Graham *et al.*, 2000). This is explained by a higher amorphous

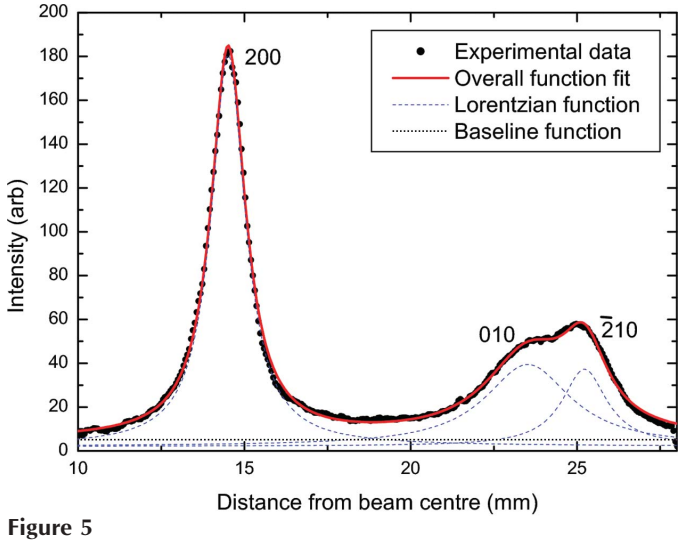

Figure 5
Example of Lorentzian function fitting to the equatorial reflections of the PBO diffraction pattern.

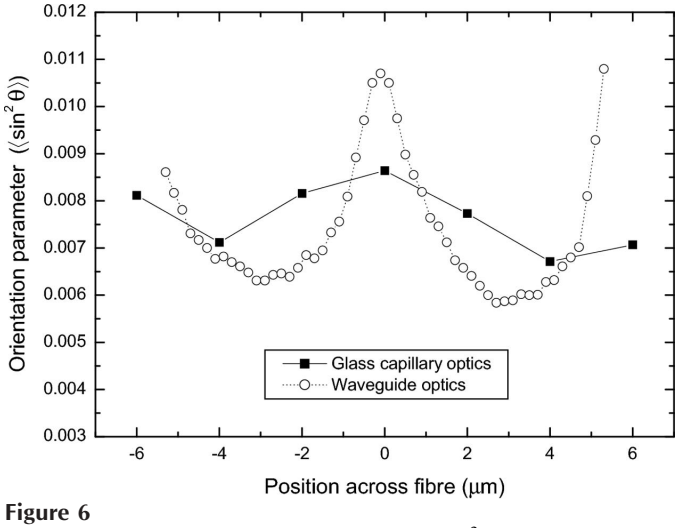

Figure 6
Skin–core variations in orientation parameter $\langle\sin^2\theta\rangle$ across single PBO fibres using glass capillary and waveguide optics.

fraction in the fibre skin (Graham *et al.*, 2000). Similarly, a μ-XRD study of PPTA fibres reports both skin and core regions of the fibre to be more disordered (Roth *et al.*, 2003). These observations are consistent with the results presented within this study on as-spun PBO fibre. The skin region of PPTA fibres is thought to consist of uniform, well packed fibrils (Panar *et al.*, 1983). This morphology is also shared by PBO as it has a similar production route and is reported to have a void-free skin layer (Kitagawa *et al.*, 1998). Thus the results shown in Fig. 6 suggest that, whilst the skin region may be more organized on a fibrillar scale, it is less organized on molecular and crystallographic scales.

3.2. Equatorial reflection intensity variations

Fig. 7 shows the radial variation in scattering intensity around the position of the 200 equatorial reflection, plotted against beam position across the fibre. The data shown was generated exclusively using waveguide optics. It demonstrates how the radial profile of the 200 reflection evolves as the fibre is scanned through the beam. The fact that there is a reduction in scattering from (200) crystal planes at the central position across the fibre indicates the existence of radial texturing. To highlight this central position, a dotted line is plotted over the data in Fig. 7. The variation in 200 scattering intensity may be explained in terms of the PBO unit cell being aligned within fibrils with the *a*-axis radially about the centre of the fibre. This textured morphology has previously been reported from SAED and XRD studies of the PBO fibre type (Kitagawa *et al.*, 1998; Davies *et al.*, 2005). A study of the PPTA fibre type using waveguide optics also reports the existence of similar texturing effects (Roth *et al.*, 2003).

Whilst Fig. 7 clearly demonstrates the existence of crystallographic texturing, it is unsuitable for a comparison of the results obtained using different beam sizes. Consequently, Fig. 8 shows the variation in the integrated intensity of the 200 equatorial reflection across the fibre width. Data collected using both waveguide and glass capillary optics are shown normalized for comparison. Both series indicate the presence of texturing through the variations in reflection intensity across the fibre. Both series also show scattering intensity to be slightly asymmetric across the fibre width. However, the variations in the glass capillary data series are less pronounced compared with the waveguide series. Therefore, similarly to the crystalline domain orientation results shown in Fig. 6, the range over which intensity varies is much less in the data collected using a larger beam size owing to the morphological averaging effect. The slight increase in scattering intensity in the proximity of the fibre centre in the waveguide series (marked with an arrow for clarity) is consistent with a rotationally disordered fibre core region. A similar result is reported for PPTA (Roth *et al.*, 2003).

3.3. Crystal lattice spacing

Fig. 9 shows the change in (200) crystal plane spacing between the skin and core regions of a single PBO fibre. If the waveguide and glass capillary data series are compared, they exhibit excellent agreement. Both series show a reduction in the spacing of the (200) crystal planes towards the centre of the fibre, of approximately the same magnitude. However, whilst the waveguide series exhibits a sharp increase around 0 μm, this feature is completely absent in the results obtained using glass capillary optics. Therefore, in this case, morphological averaging obscures an important feature when using a larger beam profile.

To interpret the morphology shown in Fig. 9, it is necessary to consider the crystallographic texturing results shown in Fig. 8. As the PBO unit-cell angle $\gamma = 101.3^\circ$ (Martin & Thomas, 1991; Fratini *et al.*, 1989), the (200) crystal planes may be considered as azimuthally oriented about the fibre axis. To clarify this, consider that if the *a*-axis of a given unit cell within the fibre is radially oriented then, according to the fixed angular relationships between lattice directions, a (200) crystal plane is perpendicular to this by approximately ±10°. The

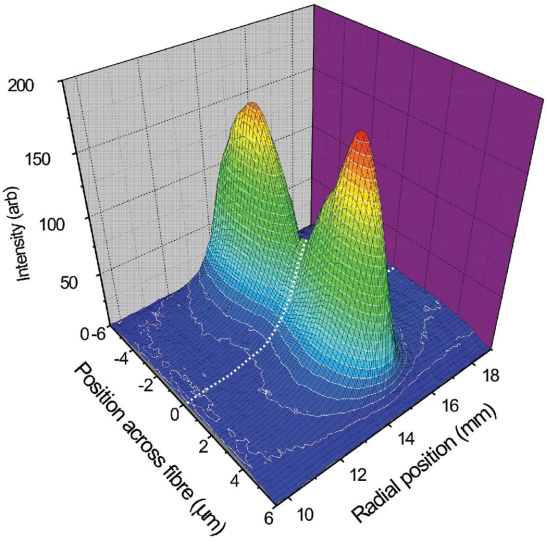

Figure 7
Radial variation in scattering intensity around the position of the 200 equatorial reflection across the fibre width.

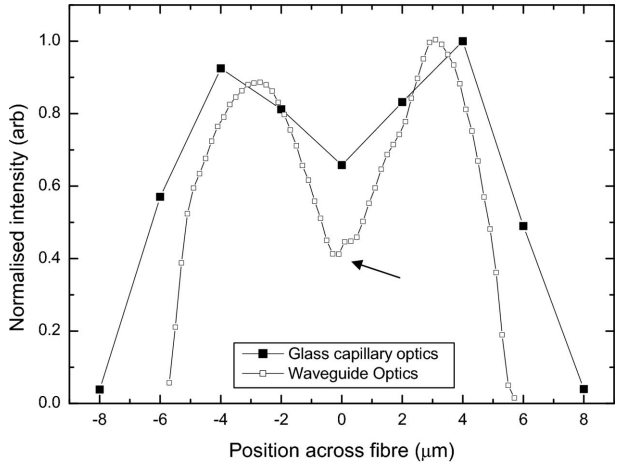

Figure 8
Variations in the integrated intensity of the 200 equatorial reflection across the fibre width calculated using glass capillary and waveguide optics.

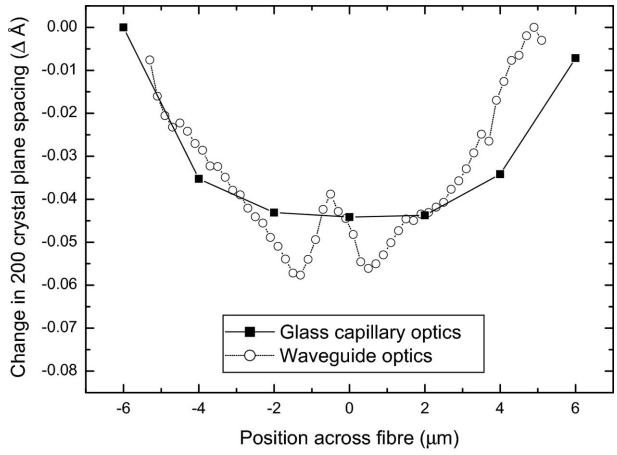

Figure 9
Variation in (200) crystal plane spacing (*d*-spacing) across a single fibre determined using glass capillary and waveguide optics.

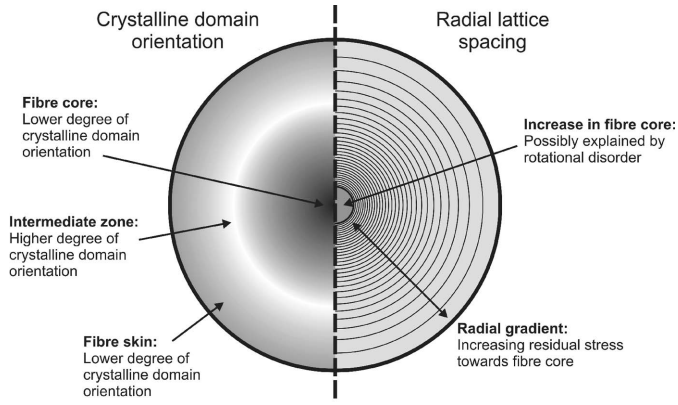

Figure 10
Summary of study results showing how the degree of crystalline domain orientation and (200) crystal plane spacing vary with radial distance along the fibre cross section.

approximation to an azimuthal orientation of (200) crystal planes becomes valid if the distribution in radial orientation is also considered (Davies *et al.*, 2005). With this in mind, the (200) crystal plane spacing shown in Fig. 9 therefore refers to a radial spacing of the PBO crystal lattice. In both the waveguide and glass capillary results the radial spacing decreases towards the centre of the fibre, with a slight increase around the 0 μm position only apparent in the data collected using waveguide optics. In the absence of external forces, this distortion of the crystal lattice can be explained in terms of residual stresses following coagulation. The fact that residual stresses have previously been observed in the PBO fibre type through transmission electron microscopy supports this hypothesis (Krause *et al.*, 1988).

A possible mechanism can be proposed for the introduction of residual stresses. During spinning, the PBO dope is extruded under very high pressure as a consequence of the high degree of dope viscosity. Thus, during extrusion, the formed fibre experiences radial compression with molecular chains at non-equilibrium spacings. As the fibre passes through the air gap prior to coagulation, the absence of the constricting die walls allows the onset of structural relaxation. However, subsequent coagulation rapidly 'freezes' the fibre structure, resulting in a radial gradient in lattice spacing (owing to the relaxation gradient). This process may be aided by the lack of inter-chain interactions in PBO, where there are only van der Waals forces between chains. A similar proposal has been used to explain the introduction of residual stress in PPTA fibres (Rao *et al.*, 2001). It is thought that relatively high rates of coagulation cause 'freezing' of the PPTA fibre structure with chains in a state of non-equilibrium (Rao *et al.*, 2001).

The increase in lattice spacing at the centre of the fibre (around the 0 μm position) can be explained through a rotationally disordered core. The existence of rotational disorder in the PBO fibre core region is already suggested from Fig. 8. Furthermore, a study by Roth *et al.* (2003) also reports an increase in rotational disorder in the fibre core region of the PPTA fibre type (Roth *et al.*, 2003). Based upon this, the (200) crystal planes may no longer indicate radial lattice spacings exclusively. Consequently, an increase in apparent lattice spacing could be reasonably expected. The existence of this distinct inner core region is also in agreement with previous AFM observations (Li *et al.*, 1993). This reports a similar 1.4 μm-diameter core region in the centre of the PPTA fibre type (Li *et al.*, 1993). The core position in this case correlates with the position of maximum orientation parameter in Fig. 6. Thus the geometric origin of influence for both orientation and lattice distortion appears identical.

Fig. 10 summarizes the results of this study. It demonstrates how the degree of crystalline domain orientation and (200) crystal plane spacing vary with radial distance along the fibre cross section. Differences in both parameters are shown in terms of the skin–core variations shown in Figs. 6 and 9. This schematic comparison highlights the fact that there is little correlation between the degree of crystalline domain orientation and the variation in radial lattice spacing. Thus, whilst the geometrical origin of influence for both parameters appears the same, the core regions do not share similar dimensions. This suggests that such variations can occur relatively independently between different length scales. For example, radial lattice spacing is primarily dictated by forces operating on a molecular level, such as chain packing influences. By contrast, crystalline domain orientation can be influenced by motions on a fibrillar level, such as post-extrusion processing.

4. Conclusions

The data presented within this study demonstrate the importance of beam size on experimental results. Similar trends are evident between all series and, where appropriate, the results have comparable average values. Consequently a direct comparison of morphological parameters determined using different beam sizes is valid. However, important features are obscured with larger beam sizes owing to morphological averaging. Extreme values and localized variations are effectively 'smoothed out'. Consequently the fibre appears as

artificially more homogeneous. In the calculation of orientation parameter and 200 reflection intensity, this leads to the apparent difference between skin and core regions being reduced. In terms of (200) crystal plane spacings, this causes important features to be completely absent from the averaged data. Such demonstrations highlight the fact that beam size is an important parameter in μ-XRD experiments and needs consideration during data interpretation. Furthermore, the use of submicrometre beams is invaluable for probing skin–core fibre morphology in detail.

The authors thank Toyobo (Japan) for the supply of PBO fibre used in this study. The waveguide was developed at the Budker Institute of Nuclear Physics (Novosibirsk, Russia) within the context of a collaboration with Sincrotrone Trieste. Thanks are also extended to Mr I. Brough at the Manchester Materials Science Centre for the use of the Field Emission Gun Scanning Electron Microscope.

References

Baltussen, J. J. M. & Northolt, M. G. (1999). *Polymer*, **40**, 6113–6124.
Choe, E. W. & Kim, S. N. (1981). *Macromolecules*, **14**, 920–924.
David, C., Noehammer, B. & Ziegler, E. (2002). *Microelectron. Eng.* **61–62**, 987–992.
Davies, R. J., Eichhorn, S. J., Riekel, C. & Young, R. J. (2005). *Polymer*, **46**, 1935–1942.
Davies, R. J., Montes-Moran, M. A., Riekel, C. & Young, R. J. (2001). *J. Mater. Sci.* **36**, 3079–3087.
Davies, R. J., Montes-Moran, M. A., Riekel, C. & Young, R. J. (2003). *J. Mater. Sci.* **38**, 2105–2115.
Fratini, A. V., Lenhert, P. G., Resch, T. J. & Adams, W. W. (1989). *Mater. Res. Symp. Proc.* **134**, 431.
Graham, J. F., McCague, C., Warren, O. L. & Norton, P. R. (2000). *Polym. Commun.* **41**, 4761–4764.
Hammersley, A. P., Svensson, S. O. & Thompson, A. (1994). *Nucl. Instrum. Methods*, **346**, 312–321.
Hammersley, A. P., Svensson, S. O., Thompson, A., Graafsma, H., Kvick, Å. & Moy, J. P. (1995). *Rev. Sci. Instrum.* **66**, 2729–2733.
Hignette, O., Cloetens, P., Lee, W. K., Ludwig, W. & Rostaign, G. (2003). *J. Phys. IV Fr.* **104**, 231–234.
Jark, W., DiFonzo, S., Lagomarsino, S., Cedola, A., diFabrizio, E., Bram, A. & Riekel, C. (1996). *J. Appl. Phys.* **80**, 4831–4836.
Kitagawa, T., Murase, H. & Yabuki, K. (1998). *J. Polym. Sci. Polym. Phys.* **36**, 39–48.
Kitagawa, T., Yabuki, K. & Young, R. J. (2001). *Polymer*, **42**, 2101–2112.
Krause, S. J., Haddock, T. B., Vezie, D. L., Lenhert, P. G., Hwang, W. F., Price, G. E., Helminiak, T. E., O'Brien, J. F. & Adams, W. W. (1988). *Polymer*, **29**, 1354–1364.
Kumar, S. (1990). *Enyclopedia of Composites*, Vol. 14, edited by S. M. Lee, p. 51. New York: VCH.
Lai, B., Yun, W., Maser, J., Cai, Z., Rodrigues, W., Legnini, D., Chen, Z., Krasnoperova, A. A., Vladimirsky, Y., Cerrina, F. *et al.* (1998). *X-ray Microfocusing: Applications and Techniques*, edited by I. McNulty, pp. 133–136. San Diego: SPIE.
Li, S. F. Y., McGhie, A. J. & Tang, S. L. (1993). *Polymer*, **34**, 4573–4575.
Martin, D. C. & Thomas, E. L. (1991). *Macromolecules*, **24**, 2450–2460.
Morgan, R. J., Pruneda, C. O. & Steele, W. J. (1983). *J. Polym. Sci. Polym. Phys.* **21**, 1757–1783.
Muller, M., Riekel, C., Vuong, R. & Chanzy, H. (2000). *Polymer*, **41**, 2627–2632.
Northolt, M. G. (1980). *Polymer*, **21**, 1199–1204.
Northolt, M. G. & VanAartsen, J. J. (1977). *J. Polym. Sci. Polym. Symp.* **58**, 283–296.
Panar, M., Avakian, P., Blume, R. C., Gardner, K. H., Gierke, T. D. & Yang, H. H. (1983). *J. Polym. Sci. Polym. Phys.* **21**, 1955–1969.
Rao, Y., Waddon, A. J. & Farris, R. J. (2001). *Polymer*, **42**, 5937–5946.
Rebouillat, S., Peng, J. C. M. & Donnet, J. B. (1999). *Polymer*, **40**, 7341–7350.
Riekel, C., Dieing, T., Engstrom, P., Vincze, L., Martin, C. & Mahendrasingam, A. (1999). *Macromolecules*, **32**, 7859–7865.
Roth, S., Burghammer, M., Janotta, A. & Riekel, C. (2003). *Macromolecules*, **36**, 1585–1593.
Wolfe, J. F. (1988). *Encyclopedia of Polymer Science and Engineering*, Vol. 11, edited by H. F. Mark, p. 601. New York: Wiley.
Young, R. J., Lu, D., Day, R. J., Knoff, W. F. & Harris, H. A. (1992). *J. Mater. Sci.* **27**, 5431–5440.